Figure 2

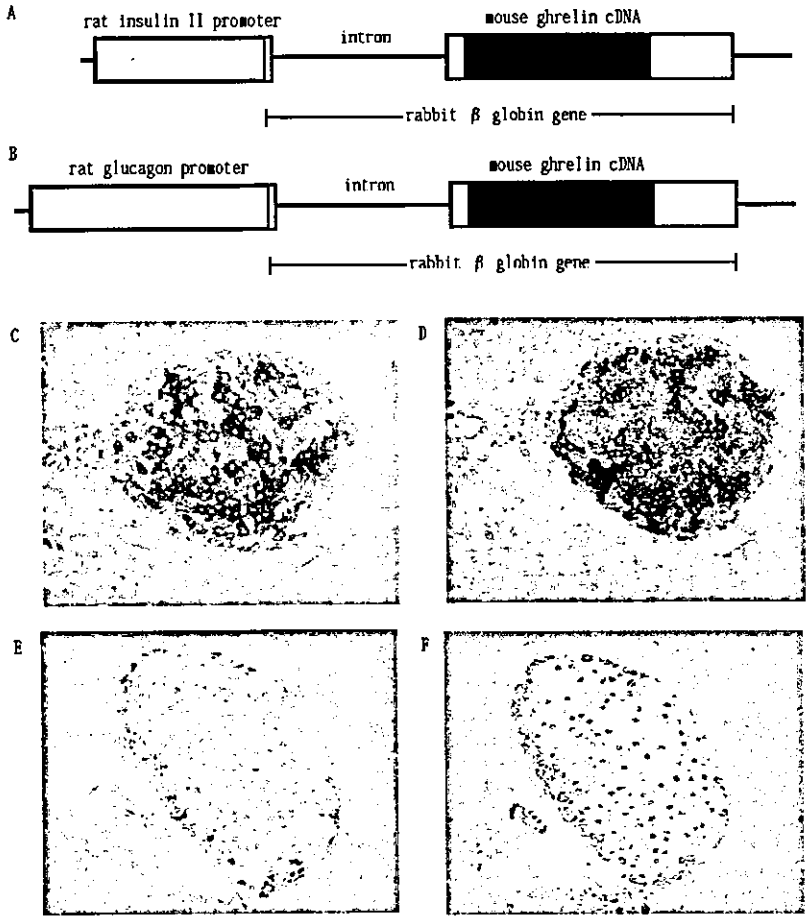
A
rat insulin II promoter
intron
mouse ghrelin cDNA
rabbit β globin gene
B
rat glucagon promoter
intron
mouse ghrelin cDNA
rabbit β globin gene
C
D
E
F

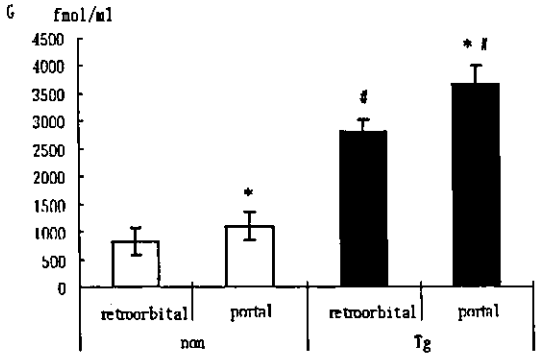
G
fmol/ml
4500
4000
3500
3000
2500
2000
1500
1000
500
0
retroorbital
portal
retroorbital
portal
non
Tg

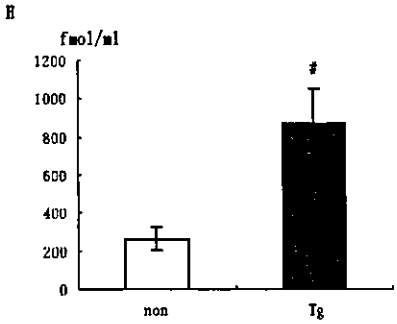
H
fmol/ml
1200
1000
800
600
400
200
0
non
Tg

13

Figure 3

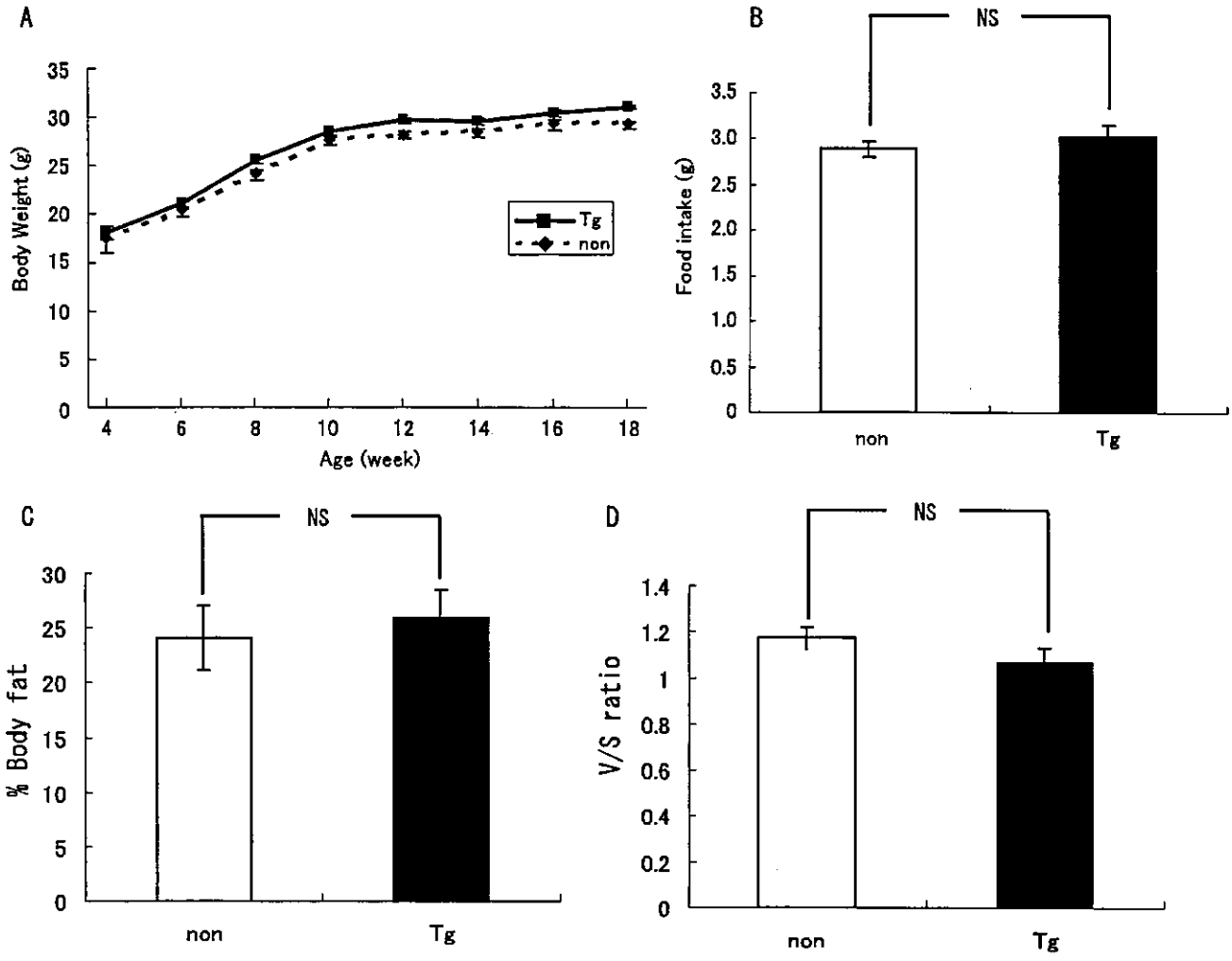
A
Body Weight (g)
Age (week)
Tg
non
B
NS
Food intake (g)
non
Tg
C
NS
% Body fat
non
Tg
D
NS
V/S ratio
non
Tg

Figure 4

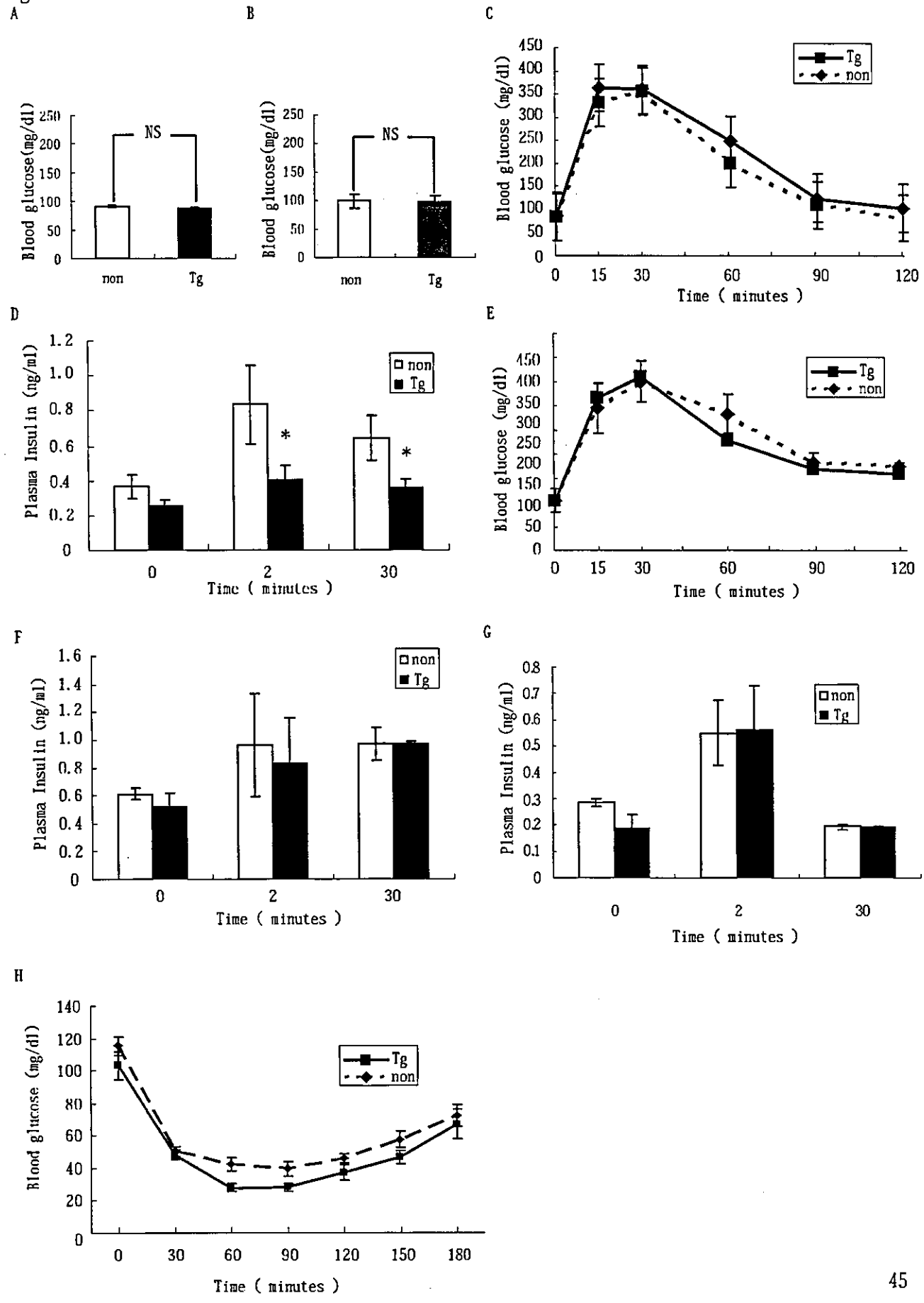
A
B
C
Blood glucose(mg/dl)
NS
non
Tg
Blood glucose (mg/dl)
Time (minutes)
D
E
Plasma Insulin (ng/ml)
Time (minutes)
F
G
H
Time (mimutes)

45

Figure 5

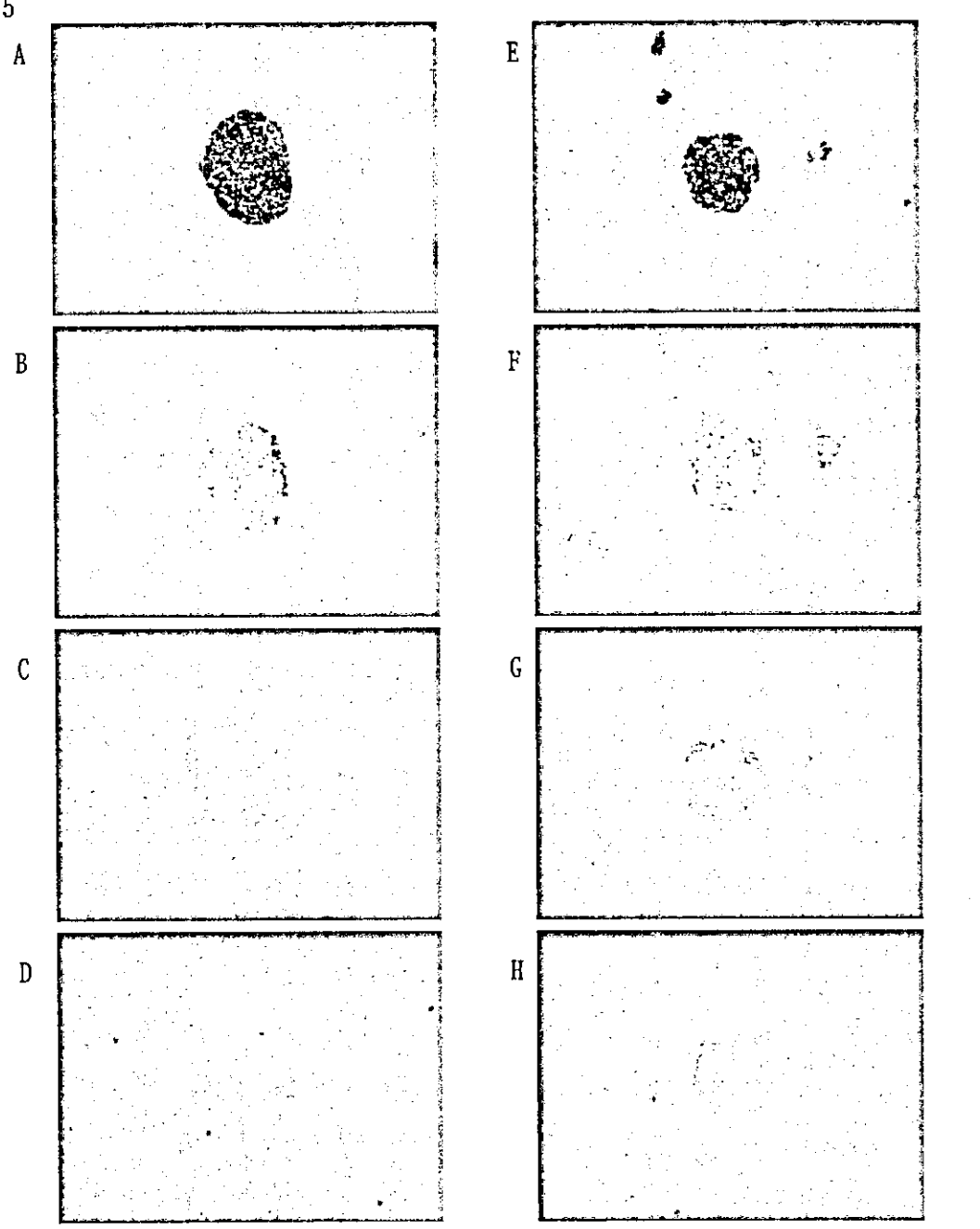
A
E
B
F
C
G
D
H

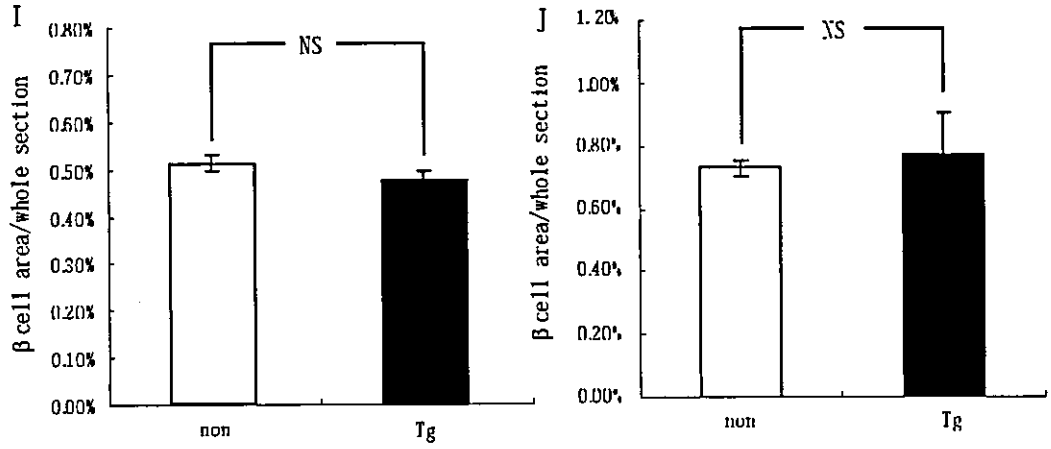
I
β cell area/whole section
0.80%
0.70%
0.60%
0.50%
0.40%
0.30%
0.20%
0.10%
0.00%
NS
non
Tg
J
β cell area/whole section
1.20%
1.00%
0.80%
0.60%
0.40%
0.20%
0.00%
NS
non
Tg

46

Figure 6

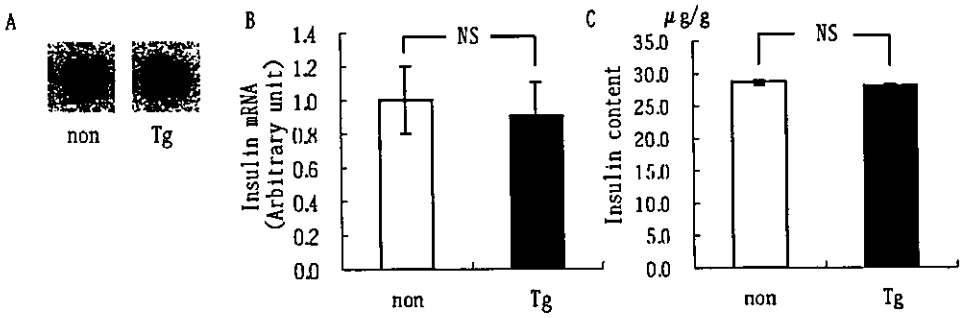
A
non
Tg
B
Insulin mRNA (Arbitrary unit)
1.4
1.2
1.0
0.8
0.6
0.4
0.2
0.0
NS
non
Tg
C
μg/g
Insulin content
35.0
30.0
25.0
20.0
15.0
10.0
5.0
0.0
NS
non
Tg

47

Figure 7

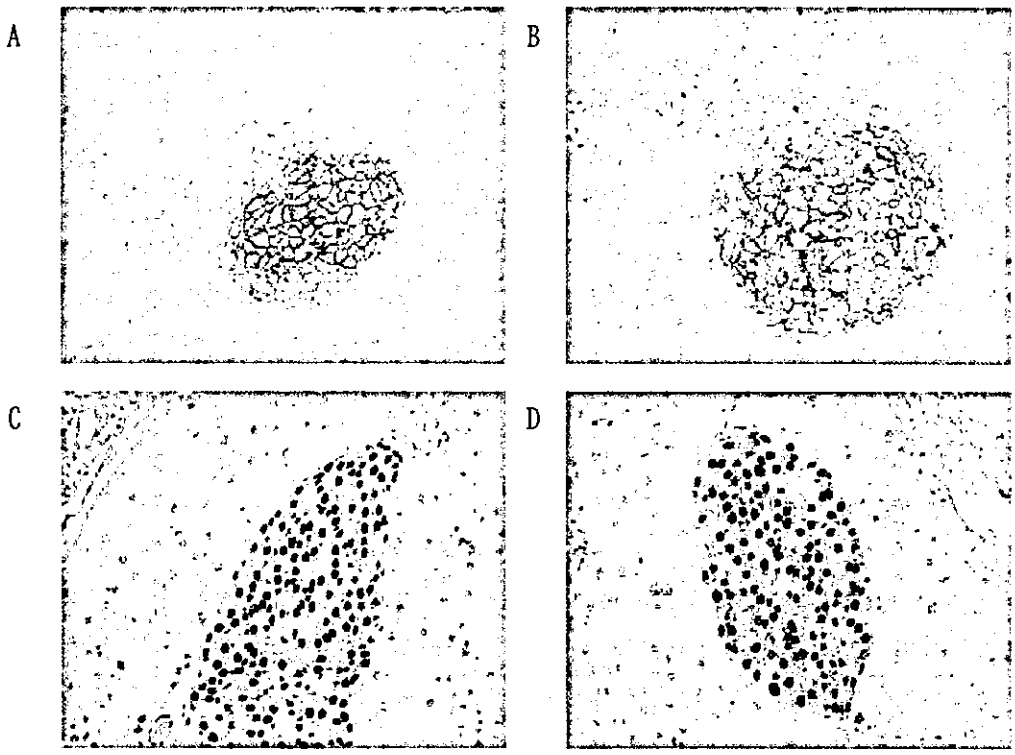

48

Figure 8

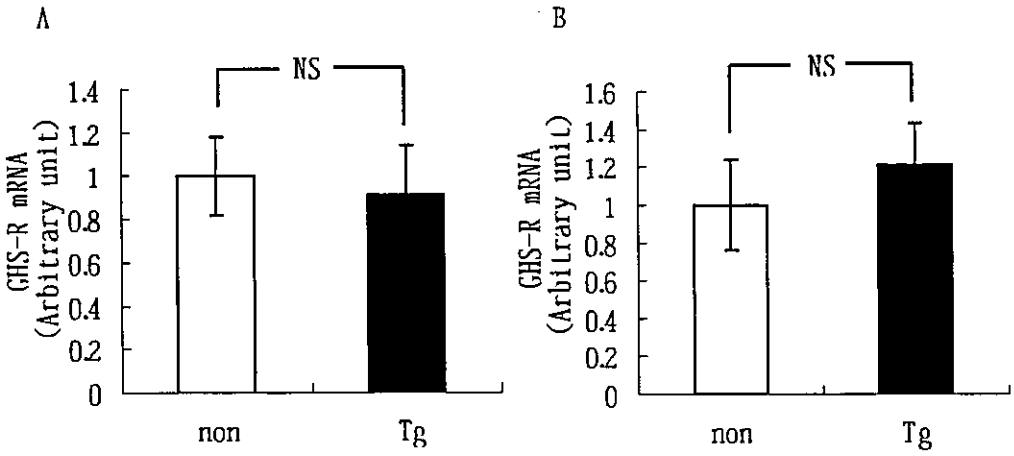
A
NS
GHS-R mRNA
(Arbitrary unit)
1.4
1.2
1
0.8
0.6
0.4
0.2
0
non
Tg
B
NS
GHS-R mRNA
(Arbitrary unit)
1.6
1.4
1.2
1
0.8
0.6
0.4
0.2
0
non
Tg

Figure 9

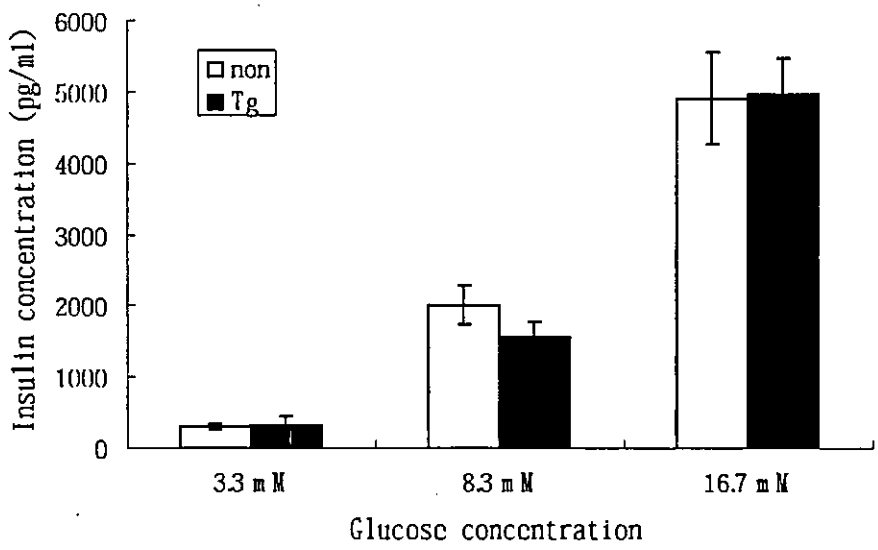
Insulin concentration (pg/ml)
6000
5000
4000
3000
2000
1000
0
non
Tg
3.3 mM
8.3 mM
16.7 mM
Glucose concentration

Spatio-Resolved Hyperbranched Graft Polymerized Surfaces by Iniferter-Based Photograft Copolymerization

Yasuhide Nakayama, Mika Sudo, Kingo Uchida, and Takehisa Matsuda

Department of Bioengineering, National Cardiovascular Center Research Institute, Fujishiro-dai 5-7-1, Suita, Osaka 565-8565, Japan, Department of Materials Chemistry, Faculty of Science and Technology, Ryukoku University, Otsu, Shiga 520-2194, Japan, and Department of Biomedical Engineering, Graduate School of Medicine, Kyushu University, 3-1-1 Maidashi, Higashi-ku, Fukuoka 812-8582, Japan

Langmuir®
The ACS Journal of Surfaces and Colloids

Reprinted from
Volume 18, Number 7, Pages 2601–2606

Spatio-Resolved Hyperbranched Graft Polymerized Surfaces by Iniferter-Based Photograft Copolymerization

Yasuhide Nakayama,[†] Mika Sudo,[†,‡] Kingo Uchida,[‡] and Takehisa Matsuda*[,§]

Department of Bioengineering, National Cardiovascular Center Research Institute, Fujishiro-dai 5-7-1, Suita, Osaka 565-8565, Japan, Department of Materials Chemistry, Faculty of Science and Technology, Ryukoku University, Otsu, Shiga 520-2194, Japan, and Department of Biomedical Engineering, Graduate School of Medicine, Kyushu University, 3-1-1 Maidashi, Higashi-ku, Fukuoka 812-8582, Japan

Received September 10, 2001. In Final Form: December 7, 2001

Two different types of three-generation hyperbranched graft surfaces with parent chain (stem), daughter chain (branch chain), and granddaughter chain (twig chain) were sequentially prepared by iniferter (*ini*tiator–trans*fer* agent–*ter*minator)-based quasi-living radical graft copolymerization using photolysis of the benzyl *N,N*-diethyldithiocarbamate (DC) group. The graft copolymerization of chloromethylstyrene (CMS) with *N,N*-dimethylacrylamide (DMAAm) or *N,N*-dimethylaminoethyl methacrylate (DMAEMA) was initiated on DC-derivatized surfaces under ultraviolet irradiation, followed by dithiocarbamylation on CMS units in the graft copolymer chains. The repeated cycles of photopolymerization/dithiocarbamylation provided successively higher generations of graft architectures. The stepwise progress of the branching stage was evidenced with changes in surface elemental composition and wettability and visualized by dye staining. From the typical force-versus-distance curves obtained by atomic force microscope measurement, some structural information of graft polymers was estimated.

Introduction

Precise architecture of surface graft chains may be needed for prevention of biocolloidal adsorption and adhesion in biomedical applications. Conventional radical graft polymerization techniques cannot control molecular parameters such as chain length and chain shape including block and branching due to the high reactivities of free radicals.[1] However, recent progress in the controlled radical reactivity technique at propagating chain ends,[2–4] including nitroxide-mediated stable free radical polymerization (SFRP),[2,5–8] atom transfer radical polymerization (ATRP),[3,9–12] and reversible addition–fragmentation chain transfer polymerization,[13] has enabled the design of precise and elegant macromolecular architectures.[14–20] Highly branched or hyperbranched polymers have drawn the attention of various research groups for 10 years, and a variety of hyperbranched polymers have been prepared.[21–34] The majority of hyperbranched polymers have been made using step growth polycondensation reactions of AB_2 type monomers, where A and B represent two different functional groups. On the other hand, on surface polymerization few hyperbranched polymer surfaces were prepared.

* To whom correspondence should be addressed. Telephone: (+81) 92-642-6210. Fax: (+81) 92-642-6212. E-mail: matsuda@med.kyushu-u.ac.jp.

† National Cardiovascular Center Research Institute.

‡ Ryukoku University.

§ Kyushu University.

(1) Moad, G.; Solomon, D. H. *The chemistry of free-radical polymerization*; Pergamon: Oxford, U.K., 1995.

(2) *Controlled radical polymerization*; Matyjaszewski, K., Ed.; ACS Symposium Series 685; American Chemical Society: Washington, DC, 1998.

(3) Sawamoto, M.; Kamigaito, M. In *Polymer Synthesis*; Materials Science and Technology Series; VCH–Wiley: Weinheim, 1998; Chapter 1.

(4) Otsu, T.; Matsumoto, A. *Adv. Polym. Sci.* **1998**, *136*, 75–137.

(5) Georges, M. K.; Veregin, R. P. N.; Kazmaier, P. M.; Hamer, G. K. *Macromolecules* **1993**, *26*, 2987.

(6) Davis, T. P.; Kukulj, D.; Haddleton, D. M.; Maloney, D. R. *Trends Polym. Sci.* **1995**, *3*, 365.

(7) Sawamoto, M.; Kamigaito, M. *Trends Polym. Sci.* **1996**, *4*, 183.

(8) Hawker, C. J. *Trends Polym. Sci.* **1996**, *4*, 456.

(9) Kato, M.; Kamigaito, M.; Sawamoto, M.; Higashimura, T. *Macromolecules* **1995**, *28*, 1721.

(10) Wang, J. S.; Matyjaszewski, K. *J. Am. Chem. Soc.* **1995**, *117*, 5614.

(11) Haddleton, D. M.; Jasieczek, C. B.; Hannon, M.; Shooter, A. *Macromolecules* **1997**, *30*, 2190.

(12) Destarac, M.; Bessiere, J.-M.; Boutevin, B. *Macromol. Rapid Commun.* **1997**, *18*, 967.

(13) Chiefari, J.; Chong, Y. K.; Ercole, F.; Krstina, J.; Jeffery, J.; Le, T. P. T.; Mayadunne, R. T. A.; Meijs, G. F.; Moad, C. L.; Moad, G.; Rizzardo, E.; Thang, S. H. *Macromolecules* **1998**, *31*, 5559.

(14) Prucker, O.; Ruhe, J. *Macromolecules* **1998**, *31*, 592.

(15) Prucker, O.; Ruhe, J. *Macromolecules* **1998**, *31*, 602.

(16) Huang, X.; Wirth, M. *J. Anal. Chem.* **1997**, *69*, 4577.

(17) Yamamoto, S.; Ejaz, M.; Tsujii, Y.; Matsumoto, M.; Fukuda, T. *Macromolecules* **2000**, *33*, 5602.

(18) Jordan, R.; Ulman, A.; Kang, J. F.; Rafailovich, M. H.; Sokolov, J. *J. Am. Chem. Soc.* **1999**, *121*, 1016.

(19) Zhao, B.; Brittain, W. J. *J. Am. Chem. Soc.* **1999**, *121*, 3557.

(20) Matyjaszewski, K.; Miller, P. J.; Shukla, N.; Immaraporn, B.; Gelman, A.; Luokala, B. B.; Siclovan, T. M.; Kickelbick, G.; Vallant, T.; Hoffmann, H.; Pakula, T. *Macromolecules* **1999**, *32*, 8716.

(21) Flory, P. J. *J. Am. Chem. Soc.* **1952**, *74*, 2718.

(22) Frechet, J. M. J.; Hawker, C. J.; Gitsov, I.; Leon, J. W. *J. Macromol. Sci., Pure Appl. Chem.* **1996**, *A33*, 1399.

(23) Malmstron, E.; Hult, A. *J. Macromol. Sci., Rev. Macromol. Chem. Phys.* **1997**, *C37*, 555.

(24) Kim, Y. H. *J. Polym. Sci., Part A: Polym. Chem.* **1998**, *36*, 1685.

(25) Voit, B. *J. Polym. Sci., Part A: Polym. Chem.* **2000**, *38*, 2505.

(26) Inoue, K. *Prog. Polym. Sci.* **2000**, *25*, 453.

(27) Kim, Y. H.; Webster, O. W. *Macromolecules* **1992**, *25*, 5561.

(28) Jikei, M.; Chon, S. H.; Kakimoto, M.; Kawauchi, S.; Imase, T.; Watanabe, J. *Macromolecules* **1999**, *32*, 2061.

(29) Emrick, T.; Chang, H. T.; Frechet, J. M. J. *Macromolecules* **1999**, *32*, 6380.

(30) Yang, G.; Jikei, M.; Kakimoto, M. *Macromoleçules* **1999**, *32*, 2215.

(31) Russo, S.; Boulares, A.; da Rin, A.; Mariani, A.; Cosulich, M. E. *Macromol. Symp.* **1999**, *143*, 309.

(32) Yamanaka, K.; Jikei, M.; Kakimoto, M. *Macromolecules* **2000**, *33*, 1111.

(33) Sunder, A.; Mulhaupt, R.; Frey, H. *Macromolecules* **2000**, *33*, 309.

(34) Yan, D. Y.; Gao, C. *Macromolecules* **2000**, *33*, 7693.

10.1021/la011415g CCC: $22.00
Published on Web 02/26/2002

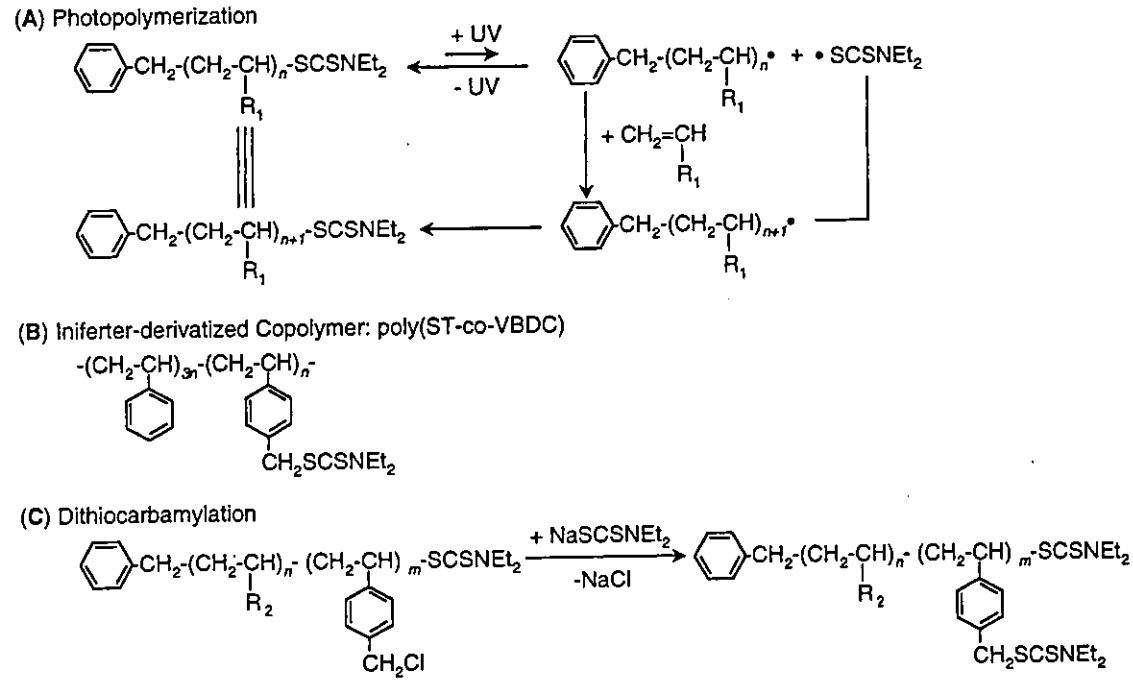

Figure 1. (A) Reaction mechanism of the iniferter-based quasi-living radical polymerization. (B) Chemical structure of dithiocarbamate group derivatized polyST (poly(ST-*co*-VBDC)). (c) Reaction mechanism of dithiocarbamylation of chloromethylstyrene group derivatized polymer.

Our attempt to design a precision surface graft architecture utilized photochemistry of *N,N*-diethyldithiocabamate (DC), by which reversible transformation between an active and a dormant species at a propagating end is strictly controlled, leading to quasi-living polymerization.[35-39] This iniferter polymerization method (Figure 1A), which was first developed for controlled macromolecular architecture in solution by Otsu et al.[40,41] in the early 1980s and proceeds during ultraviolet (UV) irradiation at room temperature, is particularly beneficial to surface functionalization on fabricated biomedical devices. Applying this iniferter-based polymerization method, the authors have designed various surface graft architectures controlling the chain length,[35] block graft chain,[35,36] gradient chain length,[35,37] and regionally graft-polymerized pattern[35,37,38] surface.

More complex but controlled hyperbranched graft architectures were prepared in our previous paper.[39] The principle is based on a sequential reaction of iniferter copolymerization with chloromethylstyrene (CMS) and subsequent dithiocarbamylation of the CMS units in the copolymers. After a stem (parent) chain was progressively propagated from an iniferter-immobilized surface, CMS units in graft chains were dithiocarbamylated. Subsequently, a branch (daughter) chain was progressively propagated on multiply derivatized iniferter units in the stem chains. The chain length for both parent and daughter chains was controlled by photoirradiation time, and the degree of branching was determined by the composition of CMS units. Figure 2 represents the schematics of the preparation of the first generation (GI) to *n*th generation (G*n*) graft architectures, in which each generation consists of two steps: dithiocarbamylation (Figure 1C) as multiple iniferter-derivatized sites on chains and subsequent iniferter polymerization (Figure 1A). Semiquantitative analysis of the graft chain lengths of stem and branch chains was assessed by the newly developed differential fluorescent technique, which convinced us that a well-controlled graft architecture was realized as designed.

In this study, as an extension of our series of studies on controlled hyperbranched graft surface designs, a three-generation branched-graft architecture consisting of parent (stem), daughter (branch), and granddaughter (twig) chains was prepared. Some insight into structural information on the graft architecture was provided by force-versus-distance curves measured by atomic force microscope (AFM).

Materials and Methods

Materials. CMS (*m*- and *p*- mixture) was obtained from Tokyo Chemical Industry Ltd. (Tokyo, Japan). Styrene (ST) was purchased from Ohken Co., Ltd. (Tokyo, Japan). Solvents and other reagents, all of which were of special reagent grade, were obtained from Wako Pure Chem. Ind. Ltd. (Osaka, Japan) and used after conventional purification. Poly(ethylene terephthalate) (PET) film was obtained from Toray Co., Ltd. (Tokyo, Japan).

DC-Derivatized PolyST Coated Surface. DC-derivatized polyST was prepared according to the method previously reported by us.[7] Briefly, the mixture of ST (0.83 g, 8.0 mmol) and vinylbenzyl *N,N*-diethyldithiocarbamate (VBDC, *m*- and *p*-mixture, 0.53 g, 2.0 mmol) in *N,N*-dimethylformamide (13.7 mL) including AIBN ([monomer]/[initiator] = 100, molar ratio) was shaken for 3 h at 60 °C. The resulting poly(ST-*co*-VBDC) copolymer (DC-derivatized polyST) was purified by reprecipitation in a toluene−methanol system three times. The yield was 0.12 g (8.5%). The molecular weight of the polymer was estimated by gel permeation chromatography (GPC) analysis: Mn = 51 400 (PST standard, eluent $CHCl_3$). The content of DC unit in the copolymer, which was determined by ^1H NMR spectroscopy from the integral ratios between the aromatic protons (δ 6.3−7.2) and the remaining S-methylene protons (δ 4.2−4.6) of the dithio-

(35) Nakayama, Y.; Matsuda, T. *Macromolecules* **1996**, *29*, 8622.
(36) Nakayama, Y.; Matsuda, T. *Langmuir* **1999**, *15*, 5560.
(37) Higashi, J.; Nakayama, Y.; Marchant, R. E.; Matsuda, T. *Langmuir* **1999**, *15*, 2080.
(38) DeFife, K. M.; Colton, E.; Nakayama, Y.; Matsuda, T.; Anderson, J. M. *J. Biomed. Mater. Res.* **1999**, *45*, 148.
(39) Lee, H. J.; Nakayama, Y.; Matsuda, T. *Macromolecules* **1999**, *32*, 6989.
(40) Otsu, T.; Yoshida, M. *Macromol. Chem. Rapid Commun.* **1982**, *3*, 127.
(41) Otsu, T.; Yoshida, M.; Tazaki, T. *Macromol. Chem. Rapid Commun.* **1982**, *3*, 133.

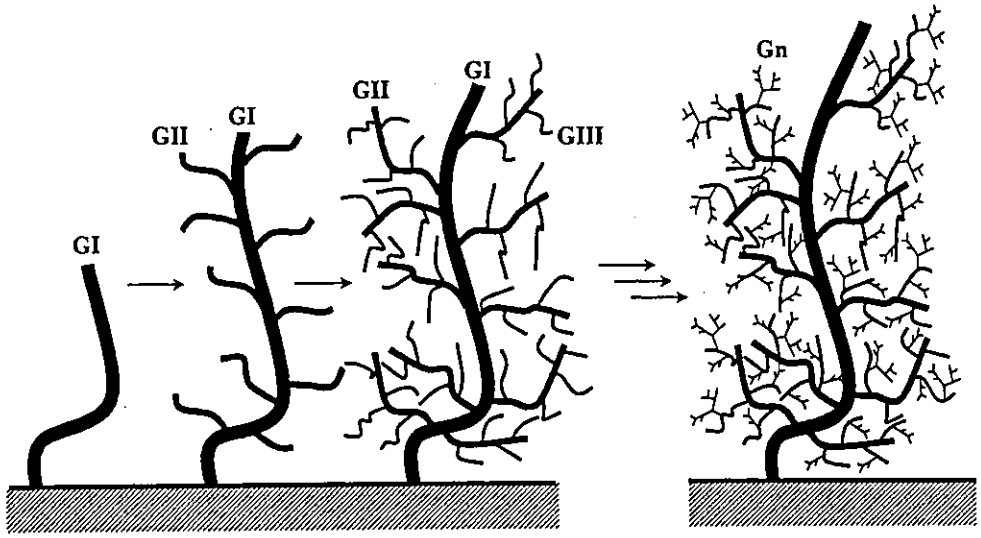

Figure 2. Schematic drawing of the first generation (GI) to *n*th generation (G*n*) graft architectures.

carbamyl group, was found to be 25.1 mol %. A toluene solution of the DC-derivatized polyST (3 mL, 1%) was coated on PET films (15 × 15 mm), which were used as substrates.

Surface Photograft Polymerization. The DC-derivatized polyST films were placed in a glass dish (diameter 30 mm), poured with 0.5 mL of a monomer-containing methanol solution (0.5 mol/dm^3), and then covered with a sapphire plate (diameter 25 mm, thickness 1 mm). Monomers used were CMS, *N,N*-dimethylacrylamide (DMAAm), and *N,N*-dimethylaminoethyl methacrylate (DMAEMA). The films were then UV-irradiated through the sapphire plate in an atmosphere of nitrogen with an ultrahigh-pressure mercury-vapor lamp (250 W, SPOT CURE250, Ushio Inc., Tokyo, Japan). The light intensity, measured with a photometer (UTR-1, Topcon, Tokyo, Japan), was 5 mW/cm^2. The temperature of the polymerized samples was maintained around 20–25 °C. The photograft-copolymerized films were rinsed with methanol and ethanol and then dried in air.

Preparation of Multiple-DC-Derivatized Film. The poly(CMS-*co*-DMAAm) or poly(CMS-*co*-DMAEMA) graft-copolymerized films were immersed in 10 mL of an ethanol solution of sodium *N,N*-diethyldithiocarbamate trihydrate (2 g, 9 mmol). After the solution was shaken for 24 h at room temperature, the multiple-DC-derivatized film was obtained. The films were thoroughly rinsed with ethanol, dried in air, and stored in a dark desiccator.

Preparation of Regionally Different Graft-Copolymerized Surface. DC-derivatized polyST film was tightly placed on a photomask with a linear opening (line width 2, 1, or 0.5 mm) (Four Leaves Co., Ltd., Osaka, Japan) and covered with a sapphire plate after being filled with a monomer-containing methanol solution. The films were irradiated through the photomask, rinsed with water and alcohol, and then dried in air. After immersion into an ethanol solution of methyl iodide, the surface-grafted films were stained with a dilute aqueous solution of rose bengal (Acid Red 94, C.I. 45440) (1.0% w/v) for visualization of the graft-copolymerized region.

Physical Measurements. All ^{1}H NMR spectra were recorded in $CDCl_3$ solution using tetramethylsilane (0 ppm) as an internal standard with a 270 MHz NMR spectrometer (GX-270, JEOL, Tokyo, Japan) at 30 °C. X-ray photoelectron spectra were taken with a Shimadzu ESCA 3400 (Kyoto, Japan) using a magnesium anode (Mg Kα radiation) at room temperature and 3 × 10^{-6} Torr (10 kV, 20 mA). Static contact angles toward deionized water were measured with a contact angle meter (Kyowa Kaimen Kagaku Co., Ltd., Tokyo, Japan) at 25 °C by the sessile drop method. Force-versus-distance curves were obtained by AFM (Dimension 3000, Digital Instruments, Santa Barbara, CA) using a probe tip with spring constant (0.12 N/m) and operated at the frequency of the approach/retract cycle of 3.2 Hz. AFM images (400 × 400 pixels) were obtained using the "height mode", which kept the force constant, and visualized using the "surface mode". Cross-sectional topography of selected regions in the AFM images was obtained with Digital Instruments software.

Results

Two different types of three-generation-graft chains were prepared from the iniferter-based copolymerization of CMS with DMAAm or DMAEMA on surfaces thinly coated with the iniferter-derivatized copolymer (poly(ST-*co*-VBDC); content of DC unit, 25 mol %) (Figure 1B). The grafted chains of DMAAm exhibited a water-soluble, nonionic character in water, whereas those of DMAEMA further subjected to quaternization exhibited a water-soluble, cationic character.

Preparation of Nonionic Hyperbranched Grafts: Stem–Branch–Twig Architecture. Iniferter-driven surface photograft copolymerization was initiated from the surface of the DC-derivatized polyST film (generation 0, G0 in Figure 3) in methanol solution containing CMS and DMAAm at a feed mole ratio of 1:20 (step I in Figure 3). After 5 min of irradiation, the treated surface was immersed into ethanol solution containing sodium *N,N*-diethyldithiocarbamate for 24 h (step II in Figure 3). X-ray photoelectron spectroscopy (XPS) measurement showed both markedly increased Cl/C and N/C ratios upon photoirradiation, and markedly reduced Cl/C and increased S/C were observed upon dithiocarbamylation (Figure 3A). These indicate that CMS–DMAAm graft-copolymerized chains as the stem chains were produced on the treated surface (stem architecture: first generation (GI), **b** in Figure 3) and then on multiple-DC-derivatized CMS units (**c** in Figure 3). In a separate solution experiment using benzyl *N,N*-diethyldithiocarbamate as a soluble iniferter, the composition of copolymer, produced under the same conditions as the surface graft copolymerization mentioned above, was found to be approximately 20 mol % for polyCMS (data not shown). This suggests that the graft chain was composed of one CMS unit per five monomer units on an average.

The successive sequential procedure of photopolymerization (step III in Figure 3) and dithiocarbamylation (step IV) under the same conditions employed for the stem architecture resulted in the same trend for the changes in Cl/C and S/C ratios (Figure 3A). These indicate that branched graft chains were produced (branch architecture: second generation (GII), **d** in Figure 3) followed by multiple-DC-derivatized CMS units (**e** in Figure 3).

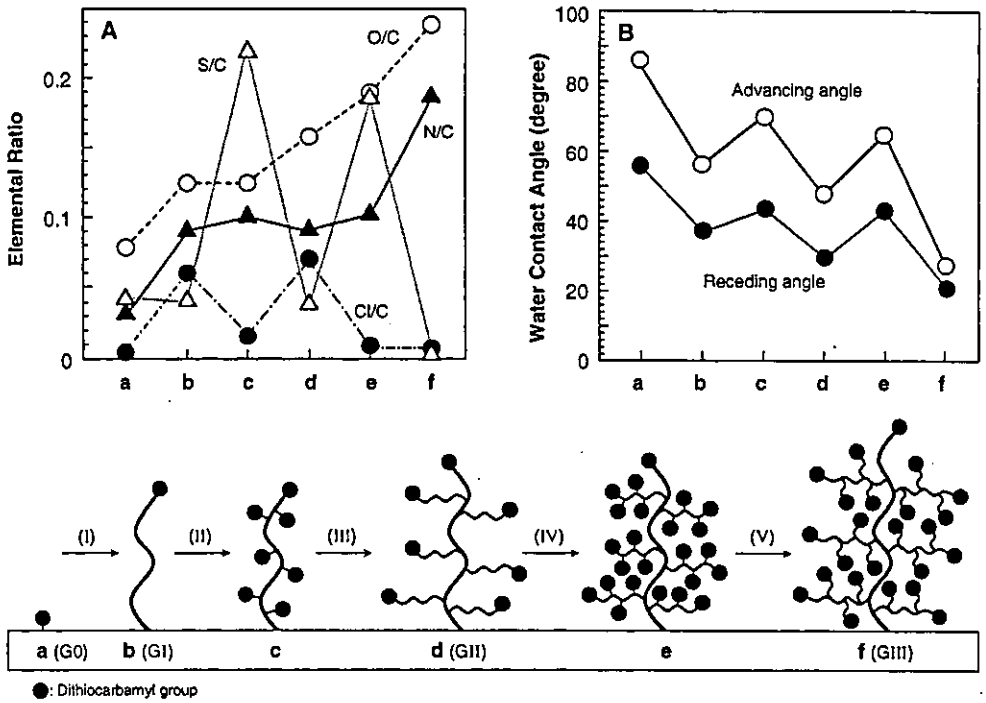

Figure 3. (A) Elemental ratio in XPS measurements and (B) water contact angle changes in the sequential progress of the branching stage by the alternate reactions of photograft copolymerization and dithiocarbamylation from the nongrafted DC-derivatized surface (G0) to the third-generation surface (GIII) and schematic drawing of the stage progress.

Photoirradiation on such treated film in DMAAm aqueous solution (step V) resulted in markedly increased O/C and N/C ratios close to the theoretical value (0.20) whereas little significant detection of Cl and S atoms was observed, indicating that polyDMAAm was grafted on branched chains (twig architecture: third generation (GIII), **f** in Figure 3).

Figure 3A,B summarizes the changes in relative elemental intensity to carbon atom and water contact angle as a function of a repeated series of photopolymerization and dithiocarbamylation. The water contact angles, both advancing and receding angle, synchronously decreased upon photopolymerization probably due to the hydrophilic PDMAAm unit but increased upon dithiocarbamylation due to the hydrophobic component of the DC unit.

Regionally Different Third-Generation-Graft Architectured Surface. The DC-derivatized surface with regionally different hypergeneration-graft architectures (the coated surface as previously mentioned) was sequentially prepared from CMS and cationic monomer, DMAEMA, using photomasks with different line widths (2, 1, and 0.5 mm). The conditions of polymerization and dithiocarbamylation were the same as those for PDMAAm hyperbranched grafts mentioned above. After photopolymerization through a photomask tightly placed on the surface, quaternization of the DMAEMA unit was carried out with methyliodide. These sequential reactions using different-sized photomasks were repeated three times. First, the stem architectured surface was prepared in a 2 mm striped pattern (GI) on the DC-derivatized surface (G0). Second, the GII surface was created with a 1 mm striped pattern on the GI grafted region, and last, the GIII surface was created with a 0.5 mm striped pattern on the GII grafted region. Rose bengal (anionic dye) staining after quaternization clearly differentiated the sequential formation of the regionally different multigeneration-graft architectures as shown in Figure 4. It was apparent that the qualitative color intensity of stained areas was in the order of GIII > GII > GI ≫ G0 (nontreated).

Force-versus-Distance Curve with the AFM. To characterize the nature and structure in water of the prepared regionally different multigeneration-graft architecture shown in Figure 4, force-versus-distance (f–d) curves using an atomic force microscope were determined in water between the grafted layer and the AFM silicone nitride probe tip. There was a marked difference in the f–d curves between nongrafted and grafted surfaces (Figure 5). When the tip was lowered to contact with the nongrafted (G0) surface, the repulsive force was generated as a linear function of tip distance (note that this is due to the enforced bending of a cantilever upon pushing down to the surface; theoretically, a very sharp repulsion force should be observed for nondeformable surfaces if the cantilever does not bend upon high loading) (Figure 5A). There was no appreciable hysteresis between approaching and retracting traces, indicating that there was little appreciable detachment force usually observed for the f–d curve of the retracting trace on hydrophobic surfaces.

On the other hand, for the GI surface, a slightly exponential f–d curve was found for the approaching trace and hysteresis between the approaching and retracting traces was observed, indicating the formation of graft-polymerized layer (Figure 5B-1). The graft density was estimated to one chain per 20–30 nm^2 (~0.04 chain/nm^2) from our recent AFM study.[42] When the cantilever tip was sufficiently pushed down on the surface, the f–d curves for both traces became identical. The separation point of the f–d curves of these traces was conveniently defined as the completely compressed state generated by enforced loading. The repulsive interaction distance between the completely compressed location (position a in Figure 5B-1, top of the compressed graft layer) and the repulsion-initiating location (position b in Figure 5B-1, top of the swollen graft layer) where repulsive force is first appreciated in an approaching trace was roughly estimated as about 100 nm. In a water-swollen graft layer,

(42) Kidoaki, S.; Nakayama, Y.; Matsuda, T. *Langmuir* **2001**, *17*, 1080.

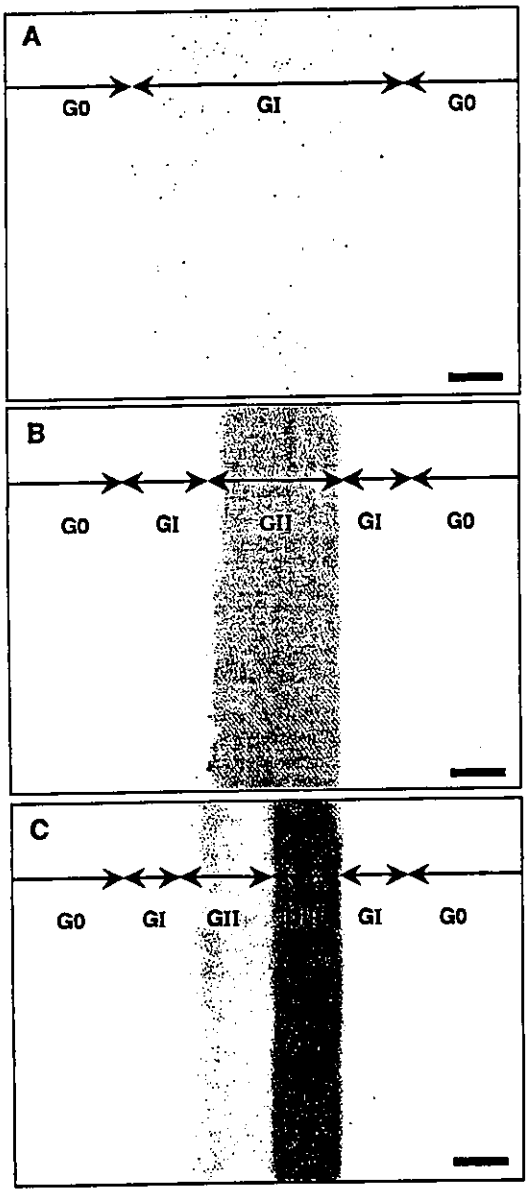

Figure 4. Visualization of the sequential progress of the branching stage by staining with rose bengal. The DC-derivatized polyST surface (G0) was graft-copolymerized with CMS and DMAEMA, followed by quaternization, while narrowing the irradiation area in each polymerization stage (A, GI; B, GI + GII; C, GI + GII + GIII) by the combination of three kinds of photomasks with linear openings (line width: 2 mm for GI, 1 mm for GII, 0.5 mm for GIII). Bar = 0.5 mm.

the real thickness of a graft layer can be defined as the sum of the compressed graft thickness and the repulsive interaction distance.[43] The compressed thickness, determined by cross-sectional analysis from AFM scanning images of the boundary area between the grafted and nongrafted regions in air, was about 30 nm (Figure 5B-2). Therefore, the real thickness was estimated as about 130 nm in the GI surface. The observed hysteresis and appreciable detachment strength in the $f-d$ curve, estimated from an adhesive jump in the retracting trace and multiple jumps, strongly suggest that the tip/graft layer interaction was complex.

The GIII surface had a much higher compression force, larger repulsion interaction force, and higher degree of hysteresis than the GI surface, indicating that although cationically charged water-soluble polyDMAEMA graft chains show steric interaction as the tip approaches the outermost layer of the graft chain in water, once the tip is forced to penetrate into a graft layer, high resistance to deformation and high detachment force are exhibited (Figure 5C-1). The real grafting thickness of the GIII surface was about 160 nm (the repulsive interaction distance, about 120 nm; the compressed thickness, 40 nm; Figure 5C-2), which was close to the value observed in the GI surface.

Discussion

The repeated cycle of iniferter-based photopolymerization and subsequent dithiocarbamylation produced a controlled graft architecture: the former reaction determines both chain length and content of precursor unit (or branching site), and the latter reaction produces iniferter on derivatization chains. Our previous study preparing a controlled graft architecture of stem and branch chains showed that chain length and degree of branching were semilinearly proportional to photoirradiation time and CMS content in the copolymers, respectively.[11] These were quantitatively determined by differential fluorescent intensity between grafted and nongrafted regions using a confocal laser scanning microscope.

This study was extended to design a more complex structure including twig (or granddaughter) chains. XPS measurement and water contact angle measurement clearly showed synchronous changes in elemental ratios and wettability, responding to photopolymerization (chain extension or branching) and dithiocarbamylation (or multiple-derivatized iniferter on a chain) (Figure 3). These results showed that such sequential reactions lead to a more hyperbranched graft architecture. Repeated cycles of photopolymerization/dithiocarbamylation progressively produced higher wettability as the generations of graft architecture progressed. In addition, higher generation graft surfaces were more densely stained, as clearly visualized on the regional multigeneration-graft architecture surface (Figure 4).

On the other hand, structural information on the graft chains in water was obtained by $f-d$ curve using the AFM (Figure 5). In principle, $f-d$ curve measurement could provide invaluable dynamic information on the structure of the swollen graft architecture upon enforced pushing-in of a tip into and pull-out from the swollen graft layer. It was apparent that as multigeneration progressed, hyperbranching of the graft architecture was enhanced, resulting in higher spacio-density of the graft chain. This may reflect the mechanical properties of swollen graft architectured surfaces. As evidenced by the comparison of $f-d$ curves of GI and GIII surfaces, with increasing generations a higher steric repulsion was observed as the probe tip made contact with the outermost graft chain and penetrated into a graft layer, both of which were derived from higher spacio-density of graft chains and configuration or topology of hyperbranching. The degree of hysteresis between approaching and retracting traces, which may be derived from the elastic pushing-out force generated upon compression of graft chains, was larger for the GIII surface than for the GI surface. In addition, detachment (or adhesive) strength was found to be larger for the GIII surface than for the GI surface. Multiple adhesion jumps were also observed. These may indicate that higher generation graft chains combine their interactions with the tip when subjected to enforced mechanical loading, resulting in the high elastic modulus of the water-swollen graft layer and a higher probability of multiple

(43) Kidoaki, S.; Ohya, S.; Nakayama, Y.; Matsuda, T. *Langmuir* **2001**, *17*, 2402.

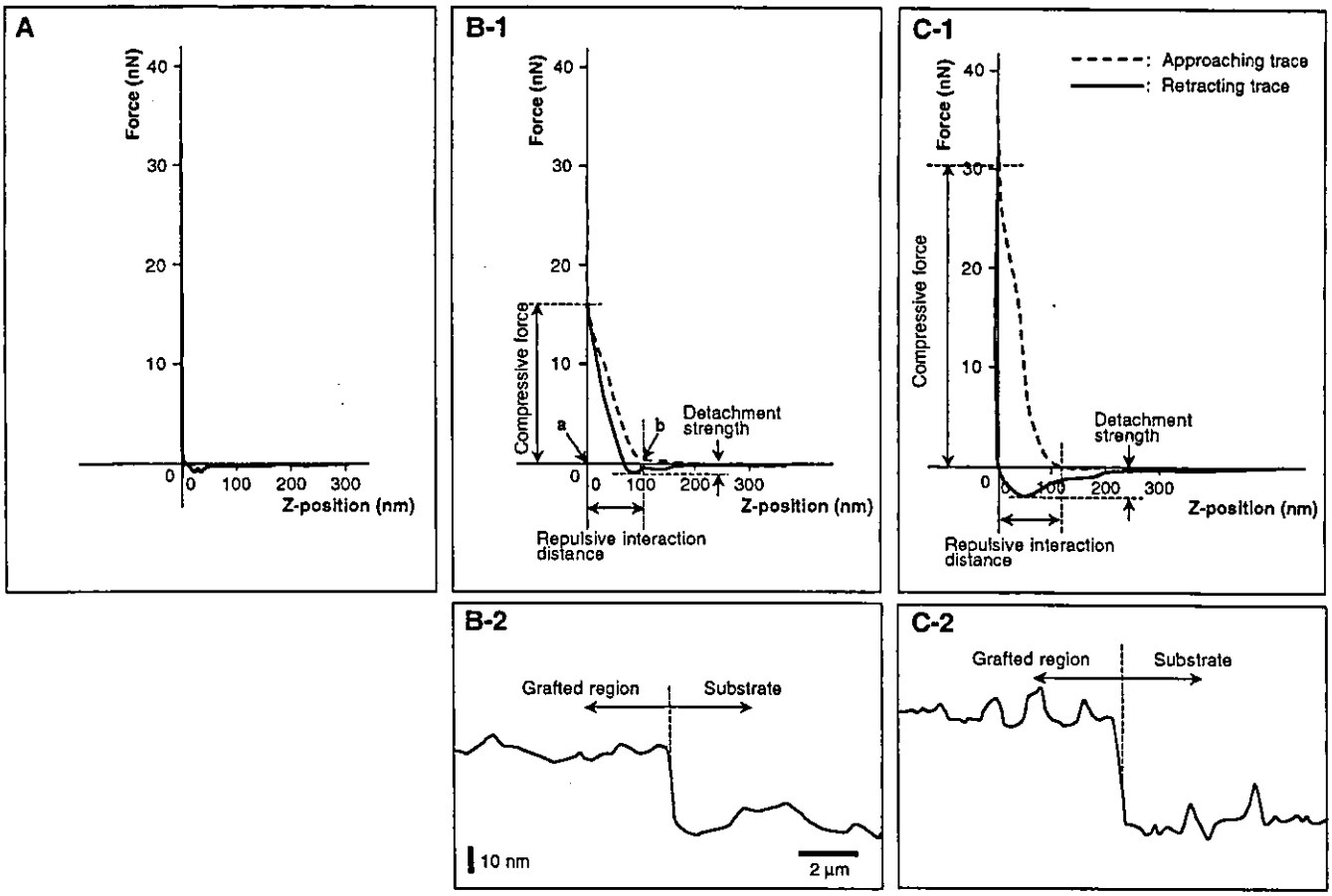

Figure 5. Force-versus-distance (*f*–*d*) curves using the atomic force microscope on (A) the DC-derivatized polyST surface and CMS–DMAEMA graft-copolymerized surfaces (B-1, GI surface; C-1, GIII surface in Figure 4). Also shown are line scan spectra for the cross-sectional topography between the boundary area of the grafted and nongrafted regions of the GI (B-2) and GIII (C-2) surfaces.

interaction of graft segments with the tip. On the other hand, between the GI and GIII surfaces there was little change in the graft thickness in water, which was defined as the sum of the repulsive interaction distances and the compressed graft thickness, as indicated in our AFM study[43] of the water-swellable graft layer. This suggests that the thickness of the graft layer did not significantly increase but the three-dimensional density of the graft chains was elevated with the progress of the graft polymerization stage.

We demonstrated a multigeneration hyperbranched graft architecture up to three generations. However, in principle, higher generation (*n*th) graft architecture is feasible upon repeated cycles of the two reactions described above (Figure 2). The spacio-resolved graft architectural method described here offers multiple choices of graft architectures in terms of main chain length, branch–branch length, chain composition, and degree of hyperbranching. In addition to the increased spacio-density of graft chains, the configuration or topology of hyperbranching may lead to different mechanical properties as compared with linear grafted chains obtained by conventional radical polymerization methods.

Acknowledgment. The authors thank Dr. Satoru Kidoaki for his very helpful technical setup and advice and Yuka Hayashi, Kanna Okuda, Kaori Shoda, and Akio Konishi for their technical support. They acknowledge the Promotion of Fundamental Studies in Health Science of the Organization for Pharmaceutical Safety and Research (OPSR) for financial support of this work under Grant No. 97-15.

LA011415G

Compliant design of artificial graft: compliance determination by new digital X-ray imaging system-based method

Hiromichi Sonoda,[1,2,3] Shin-Ichi Urayama,[4] Keiichi Takamizawa,[1] Yasuhide Nakayama,[1] Chikao Uyama,[5] Hisataka Yasui,[2] Takehisa Matsuda[3]

[1]*Department of Biomedical Engineering, National Cardiovascular Center Research Institute, 5-7-1 Fujishirodai, Suita, Osaka 565-8565, Japan*

[2]*Department of Cardiac Surgery, Graduate School of Medicine, Kyushu University, 3-1-1 Maidashi, Higashi-ku, Fukuoka 812-8582, Japan*

[3]*Department of Biomedical Engineering, Graduate School of Medicine, Kyushu University, 3-1-1 Maidashi, Higashi-ku, Fukuoka 812-8582, Japan*

[4]*Department of Investigative Radiology, National Cardiovascular Center Research Institute, 5-7-1 Fujishirodai, Suita, Osaka 565-8565, Japan*

[5]*Department of Clinical Engineering, Hiroshima International University, Gakuendai 555-36, Kurose-cho, Kamo-gun, Hiroshima 724-0695, Japan*

Received 13 August 2001; accepted 28 August 2001
Published online 23 January 2002

Abstract: The development of an artificial graft requires formulation of biomechanical design criteria. The compliance of artifical grafts, based on the intraluminal pressure-internal diameter (Pi-Di) relationship, was measured by a novel method using a digital X-ray imaging system coupled with an edge detection algorithm and a pressure transducer. The Pi-Di values were obtained from digital angiographic images under continuous inflation of a canine femoral artery anastomosed with an expanded poly(tetrafluoroethylene) (ePTFE) vascular graft as a model vessel with a pressurized contrast medium. The Di at Pi using an NIH Image software specially programmed for the entropy filter method, which enables the detection of the edge of the vessel phantoms of the images, was determined. The Pi-Di relationships showed a "J-shape" curve for the artery, a steeper line with a very low pressure-dependent distensibility for the ePTFE graft, and an intermediate curve for the anastomosis protion. The two indices for the vessel compliance, the stiffness parameter (β value) and the diameter compliance (C_d), both of which were calculated from the Pi-Di relationships, were 10.6 and 6.8%/mmHg × 10^{-2} for the artery, 164 and 0.51%/mmHg × 10^{-2} for the ePTFE, and 14.4 and 5.5%/mmHg × 10^{-2} for the anastomosis portion, respectively. This method can measure compliance at any portions of the sampling vessel in a single experiment on a real-time basis with very high accuracy, compared with conventional methods, and even in cases of intimal thickening and/or connective tissues-adhered vessels, and may serve to provide information on compliant design criteria of artificial and tissue-engineered graft. © 2002 John Wiley & Sons, Inc. J Biomed Mater Res 60: 191–195, 2002

Key words: digital X-ray imaging system; angiography technique; compliance

INTRODUCTION

Clinically used artificial vascular grafts made of plastics are generally rigid conduits. An anastomosis between a compliant host artery and a rigid vascular graft causes compliance mismatch, thereby generating hemodynamic disturbance and stress concentration, which may lead to thrombus formation at an early stage and to an excessive tissue ingrowth (neointimal hyperplasia) near the anastomosis at a later stage of implantation.[1–5] The mechanical property or the compliance of an artificial graft is a determinant of hemodynamical, pathological, and physiological functions. From a biomechanical point of view, an artificial graft exhibiting compliance matching with a native artery is essential to prevent or minimize these adverse effects, which appear to determine the fate of implanted artificial grafts. The smaller the inner diameter of artificial graft is, the more critical the compliance matching is. Precise determination of the compliance of natural arteries and artificial or tissue-engineered grafts at its regionally defined portion has long been awaited for

Correspondence to: T. Matsuda; e-mail: matsuda@med.kyushu-u.ac.jp

DOI 10.1002/jbm.10055

the formulation of criteria for biomechanical design of artificial vessels as well as for the understanding of the physiological role of compliance. To this end, our efforts have been focused on fabrication of compliant artificial grafts using an excimer laser-ablated, micropored segmented, polyurethane single tube[6,7] and coaxial double tubes.[8]

As for the determination of the compliance of arteries or artificial grafts, which requires measurement of the pressure-dependent vessel diameter, several methods have been reported: the echo-tracking method,[9,10] the loop-probe method,[11,12] the cantilever method,[2,13,14] the optical width analyzer method,[6–8,15–18] and the classical angiography technique.[19,20] Both the echo-tracking and the loop-probe methods enable us to determine the internal diameter of the vessel *in vivo* on a real-time basis: the former method, in which the diameter of blood vessels is measured from outside of the arteries, cannot be applied to echo beam-impermeable artificial grafts, and the latter one involves the insertion of a probe in an artery or an artificial graft. Both the cantilever and optical width analyzer methods can measure the external diameter of all vessels except for vessels that are tightly adhered to the surrounding tissues. On the other hand, the classical angiography technique can measure the internal diameter of the vessels both *in vivo* and *in vitro*, even for artificial grafts, the outer surface of which is heavily adhered to a surrounding tissue.

In this article, the angiography method, which was originally developed for determining blood vessel diameter on cineangiography and is based on a digital X-ray imaging system coupled with a specially designed algorithm for determination of the intraluminal edge of an artery, is modified to measure the intraluminal pressure-dependent internal diameter changes of the vessel. This method, in which accuracy of determination is essentially very high among the existing methods, can easily and accurately determine the regionally specific compliance or stiffness of a natural artery and an artificial graft and their site of anastomosis. An anstomosis model between an artery and an ePTFE graft is presented for verification of the potential applicability of this method for determining the compliance at a desired part of the host artery/artificial graft-anastomosed segment.

MATERIALS AND METHODS

An anastomosis between an artery and an artificial graft was created as follows. A femoral artery of a mongrel dog (weighing ~30 kg) was mobilized and clamped, and the anastomosis was performed with an ePTFE vascular graft (Stretch Thin Wall; W.L. Gore & Associates, Inc., Flagstaff, AZ) using a continuous 7-0 nylon suture in end-to-end fashion (~4 cm in length). The vessel segment including the anastomosis (~8 cm in length) was obtained and mounted to the holder according to the following procedure.

The measurement apparatus for determining the intraluminal pressure-internal diameter (Pi-Di) relationship is composed of a digital X-ray imaging system (Series 9600; OEC Medical Systems, Inc., Salt Lake City, UT), a pressure transducer (6M92; NEC-Sanei, Tokyo, Japan), and a custom-designed holder for mounting a vessel (Fig. 1). The X-ray booster and the image intensifier of the imaging system were positioned to obtain the optimal image size of the vessel. One end of the vessel segment was cannulated to a fixed stainless steel connector for pressure loading with a syringe pump (Truth all-round injector; Nakagawa-Seikodo Co., Ltd., Tokyo, Japan; injection rate, ~1 ml/min) and the other to a sliding connector attached to the pressure transducer. The vessel segment, after several cycles of repeated inflation and deflation of the vessel with Krebs-Ringer solution and subsequent immersion in Krebs-Ringer solution at 37°C, was gradually inflated by infusion of a contrast medium (Iomeron 350; Eisai Co., Ltd., Tokyo, Japan) up to a pressure of

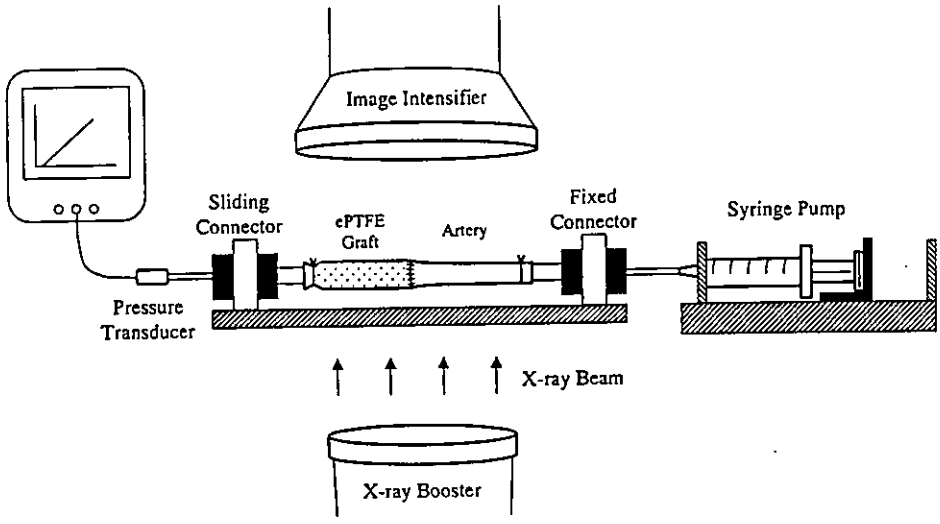

Figure 1. Schematic diagram of the system for determining the intraluminal pressure-internal diameter relationship using a digital X-ray imaging system and a pressure transducer.

~200 mmHg. The X-ray images and the pressure were recorded simultaneously. After all images were recorded (8 frames/s), the sequential images at each 5-mmHg step of pressure were sampled using a digital-video-editing software (iMovie, Version 1.0.2; Apple Computer, Inc., Cupertino, CA) and the stacked images were reconstructed using an image-processing software (NIH Image, Version 1.59, public domain software). The measurement of the internal diameter of the vessel on each image was carried out automatically with an NIH Image software programmed in its macro-language. A region of interest (ROI) in the target area of the vessel was selected on the top most image of the stacked ones. Because the edge detection procedure was performed horizontally, the vessel was positioned vertically as much as possible.

The next step was to determine precisely the intraluminal diameter. The method used here was principally based on the method originally developed for the determination of blood vessel diameter on cineangiogram using an "entropy filter" method proposed by Uyama et al.[21] The entropy filter is defined as[22]:

$$e(i) = \frac{1}{P(i)} \sum_{j=-w}^{w} g(i+j) \log \frac{g(i+j)}{P(i)} \quad (1)$$

where

$$P(i) = \sum_{j=-w}^{w} g(i+j) \quad (2)$$

Here, $e(i)$ is the entropy, $g(i)$ is the gray-level value (256 levels) at the pixel along the scanning line, and w is the scanning window width of each edge. The edge position is determined at the point in which the value of $e(i)$ is maximum at each side of the vessel's image. Scanning was carried out vertically from the top to the bottom line of ROI. When the vessel was tilted, the diameters were corrected by multiplying them with the cosine of the angle between the central line of the vessel and the vertical line of the image. The above procedures were repeated through all stacked images by the same positioned ROI. Minimal measurable ranges are ~10 μm in diameter and 0.25 mmHg in pressure. After the Pi-Di relationship was obtained, the stiffness parameter (β value) and the diameter compliance (C_d) were calculated according to the following equations.

The stiffness parameter (β value), which is an index of compliance proposed by Hayashi et al.,[18,23] was determined according to the following equation:

$$\ln(P/P_s) = \beta(D/D_s - 1) \quad (3)$$

where P is the pressure and D is the diameter at P, and P_s and D_s are the standard intraluminal pressure (100 mmHg in this study) and the internal diameter at P_s, respectively. A smaller β value indicates a more compliant vessel.

The diameter compliance (C_d) was calculated using the following formula:

$$C_d = \Delta D/(D \times \Delta P) \quad (4)$$

where D is the internal diameter of the vessel and ΔD is the diameter change associated with a ΔP (pressure increment) at the intraluminal pressure of 100 mmHg. The unit was expressed as percentage diameter change per mmHg × 10^{-2}.

RESULTS

In this study, the vertical width of a region of interest (ROI) for measuring diameter was fixed at 1 mm (~10 pixel lines). From the computer analysis of the obtained sequential pressure-dependent X-ray images, the Pi-Di relationships for the native artery, the ePTFE graft, and the anastomosis portions were simultaneously calculated in a single experiment.

Distinct digital images were obtained from the anastomosis model (Fig. 2). The Pi-Di relationship for the artery exhibited a "J-shape" curve as shown in Figure

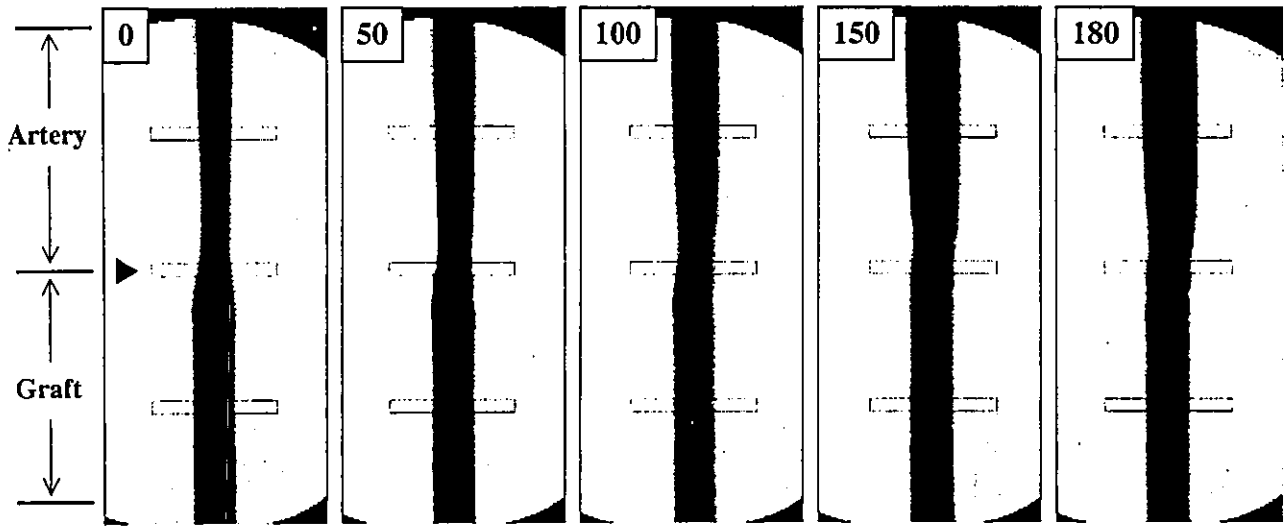

Figure 2. Changes in the digital angiographic images of the model of anastomosis between an artery and an ePTFE graft under continuous inflation with a contrast medium. The squares indicate the regions of interest (ROI) in the artery, the anastomosis portion and the graft. The arrowhead shows the position of the anastomosis. The numbers indicate the intraluminal pressures (mmHg).

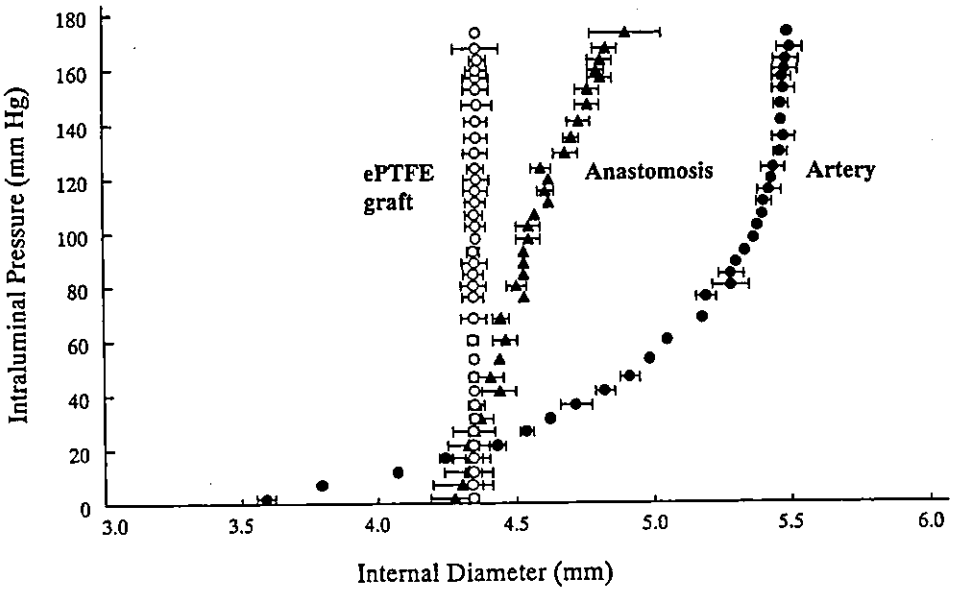

Figure 3. Intraluminal pressure-internal diameter relationships for the artery, the ePTFE graft and the anastomosis portions (mean values ± standard deviations).

3, indicating a marked increase in distensibility in the low-pressure range, followed by a gradual reduction in pressure-dependent distensibility in the physiological pressure range, and little inflation was observed in the high-pressure range. On the other hand, for the ePTFE graft, a steeper line in the Pi-Di relationship was obtained, indicating a very low pressure-dependent distensibility over the entire pressure range. For the anastomosis portion, the Pi-Di relationship exhibited an intermediate curve of those mentioned above.

The stiffness parameter (β value) and the diameter compliance (C_d), both of which were calculated from these curves, were 10.6 and 6.8%/mmHg × 10^{-2} for the artery, 164 and 0.51%/mmHg × 10^{-2} for the ePTFE graft, and 14.4 and 5.5%/mmHg × 10^{-2} for the anastomosis portion (Table I). Both values indicate that the artery is much more compliant than the ePTFE graft, and the anastomosis portion determined at an arterial portion of the anastomotic region has a compliance that is slightly reduced compared with the artery, indicating that suturing appears to reduce compliance in this particular case.

DISCUSSION

Mechanical stress field in a pulsatile-flow- and high-pressure-loaded arterial system provides a hostile environment for an implanted artificial graft. The significance of differential pressure-induced distensibility between a native artery and an anastomosed artificial graft on the fate of implanted device (i.e., patency or occlusion) has been discussed over the years. Abbott and coworkers[1-3] have suggested that the compliance mismatch between a native artery and a vascular graft is a major detrimental factor, leading to the graft failure of small-diameter vascular conduits, and that even suturing causes compliance mismatch.[14] The precise determination of the pressure-dependent diameter relationship is essential for the understanding of compliance mismatch and formulating criteria for biomechanical design of an "ideal" artificial graft in terms of mechanical compatibility or compliance matching. According to previous reports, the internal diameter of vessels has been measured mainly by using the echo-tracking method,[9,10] which enables visualization of the two-dimensional short-axis view of the artery wall and capturing of the wall movement. Although this method determines internal diameter changes of vessels even in an *in vivo* experiment, the echo beam may be impermeable to synthetic materials such as polyester-based (Dacron) or ePTFE grafts. On the other hand, the cantilever method,[2,13,14] which measures the external diameter changes of vessels by using a cantilever transducer, is inappropriate to observe an artificial graft adhered tightly to massively growing surrounding tissues.

Compliance is defined as the pressure-depending volumetric change of a vessel. As the volume of a circular tube is correlated to the internal diameter of

TABLE I
Stiffness Parameter (β Value) and Diameter Compliance Value (C_d) for Artery, ePTFE Graft, and Anastomosis

	β Value	C_d (%/mm Hg × 10^{-2})
Artery	10.6	6.8
ePTFE	164	0.51
Anastomosis	14.4	5.5

the tube, the procedure for measuring the internal diameter accurately should be most important. In the optical width analyzer method,[6–8,15–18] which we used in our previous studies, the pressure-dependent diameter changes were measured using an apparatus composed of a charge-coupled device (CCD) camera with a width analyzer and a pressure transducer, which determines the external diameter and the intraluminal pressure, respectively. However, this method has the same methodological limitation as the cantilever method: the precise diameter values are not obtained when an artery or an artificial graft is adhered to massively growing surrounding tissues.

The present method is a modified cineangiography, which applied the digital imaging system and the calculation of the internal diameter by using a specially designed algorithm and the commonly used image-processing software. The advantage of this method is that the whole-vessel (including the artificial graft) images at a given intraluminal pressure are obtained by single sampling that the spacio-dimensional accuracy is very high (errors within 10 μm) and that these data can be translated into the stiffness parameter (β value) and the diameter compliance (C_d) at any portions of the vessel (e.g., artificial graft, anastomosis, or native artery). In addition, this method can measure the compliance of the vessels that are highly adhered to surrounding tissues under *in situ* hemodynamic condition.

Previous studies reported that the β values are 5.25 to 40 for native arteries, including coronary and common carotid arteries, and ~150 for ePTFE grafts, and the C_d values are 5.9–9.8%/mmHg × 10^{-2} for native arteries and ~1.6%/mmHg × 10^{-2} for ePTFE grafts, as determined by the optical width analyzer, cantilever and loop-probe methods.[2,11–13,16,23,24] These values are found to be very close to those determined by the present method.

Once compliance is precisely determined, a more logical biomechanical design of the scaffold of artificial grafts could be realized. We are now determining the time-dependent changes in compliance of newly designed compliant artificial grafts,[8] which have been implanted up to 1 year; results of this study using the present method will be reported soon.

References

1. Abbott WM, Megerman J, Hasson JE, L'Italien G, Warnock DF. Effect of compliance mismatch on vascular graft patency. J Vasc Surg 1987;5:376–382.
2. Walden R, L'Italien GJ, Megerman J, Abbott WM. Matched elastic properties and successful arterial grafting. Arch Surg 1980;115:1166–1169.
3. Hasson JE, Magerman J, Abbott WM. Increased compliance near vascular anastomoses. J Vasc Surg 1985;2:419–423.
4. Weston MW, Rhee K, Tarbell JM. Compliance and diameter mismatch affect the wall shear rate distribution near an end-to-end anastomosis. J Biomech 1996;29:187–198.
5. Kinley CE, Marble AE. Compliance: a continuing problem with vascular grafts. J Cardiovasc Surg 1980;21:163–170.
6. Doi K, Nakayama Y, Matsuda T. Novel compliant and tissue-permeable microporous polyurethane vascular prosthesis fabricated using an excimer laser ablation technique. J Biomed Mater Res 1996;31:27–33.
7. Doi K, Matsuda T. Significance of porosity and compliance of microporous, polyurethane-based microarterial vessel on neoarterial wall regeneration. J Biomed Mater Res 1997;37:573–584.
8. Sonoda H, Takamizawa K, Nakayama Y, Yasui H, Matsuda T. Small-diameter compliant arterial graft prosthesis: Design concept of coaxial double tubular graft and its fabrication. J Biomed Mater Res 2001;55:266–276.
9. Studinger P, Lenard Z, Reneman R, Kollai M. Measurement of aortic arch distension wave with the echo-track technique. Ultrasound Med Biol 2000;26:1285–1291.
10. Isnard RN, Pannier BM, Laurent S, London GM, Diebold B, Safar ME. Pulsatile diameter and elastic modulus of the aortic arch in essential hypertension: a noninvasive study. J Am Coll Cardiol 1989;13:399–405.
11. Klein SR, Goldberg L, Miranda RM, Bosco P, Nelson RJ, White RA. Effect of suture technique on arterial anastomotic compliance. Arch Surg 1982;117:45–47.
12. White R, Goldberg L, Hirose F, Klein S, Bosco P, Miranda R, Long J, Nelson R, Shors E. Effect of healing on small internal diameter arterial graft compliance. Biomater Med Devices Artif Organs 1983;11:21–59.
13. Baird RN, Kidson IG, L'Italien GJ, Abbott WM. Dynamic compliance of arterial grafts. Am J Physiol 1977;233:H568–H572.
14. Hasson JE, Megerman J, Abbott WM. Suture technique and para-anastomotic compliance. J Vasc Surg 1986;3:591–598.
15. Takamizawa K, Hayashi K. Strain energy density function and uniform strain hypothesis for arterial mechanics. J Biomech 1987;20:7–17.
16. Hayashi K, Takamizawa K, Saito T, Kira K, Hiramatsu K, Kondo K. Elastic properties and strength of a novel small-diameter, compliant polyurethane vascular graft. J Biomed Mater Res 1989;23(A2 Suppl):229–244.
17. Takamizawa K, Hayashi K, Matsuda T. Isometric biaxial tension of smooth muscle in isolated cylindrical segments of rabbit arteries. Am J Physiol 1992;263:H30–H34.
18. Hayashi K, Nakamura T. Material test system for the evaluation of mechanical properties of biomaterials. J Biomed Mater Res 1985;19:133–144.
19. Gozna ER, Marble AE, Shaw A, Holland JG. Age-related changes in the mechanics of the aorta and pulmonary artery of man. J Appl Physiol 1974;36:407–411.
20. Dobrin PB, Mirande R, Kang S, Dong QS, Mrkvicka R. Mechanics of end-to-end artery-to-PTFE graft anastomoses. Ann Vasc Surg 1998;12:317–323.
21. Uyama C, Kita Y, Matsusita S. Optimal sampling interval and edge detection algorithm for measurement of blood vessel diameter on a cineangiogram. Invest Radiol 1993;28:1128–1133.
22. Shiozaki A. Edge extraction using entropy operator. Computer Vision, Graphics and Image Processing 1986;36:1–9.
23. Hayashi K, Handa H, Nagasawa S, Okumura A, Moritake K. Stiffness and elastic behavior of human intracranial and extracranial arteries. J Biomech 1980;13:175–184.
24. Kidson IG, Abbott WM. Low compliance and arterial graft occlusion. Circulation 1978;58(Suppl):I1–I4.